Nano Research
2023, 16(7): 9379–9386

ISSN 1998-0124 CN 11-5974/O4
https://doi.org/10.1007/s12274-023-5587-0

Research Article

Continuous synthesis of ultra-fine fiber for wearable mechanoluminescent textile

Shulong Chang[1], Yuan Deng[1], Na Li[1], Lijun Wang[1,2], Chong-Xin Shan[1] (✉), and Lin Dong[1] (✉)

[1] *Key Laboratory of Material Physics, Ministry of Education, School of Physics and Microelectronics, Zhengzhou University, Zhengzhou 450052, China*
[2] *State Key Laboratory of Luminescence and Applications, Changchun Institute of Optics, Fine Mechanics and Physics, Chinese Academy of Sciences, Changchun 130033, China*

Received: 6 January 2023 / **Revised:** 7 February 2023 / **Accepted:** 17 February 2023

ABSTRACT

Continuous mechanoluminescence (ML) fibers and fiber-woven textiles have the potential to serve as new wearable devices for sensors, healthcare, human–computer interfacing, and Internet of Things. Considering the demands on wearability and adaptability for the ML textiles, it is essential to realize the continuous synthesis of fiber, while maintaining a desired small diameter. Here, we develop a novel adhere-coating method to fabricate ML composite fiber, consisting of a thin polyurethane (PU) core and ZnS:Cu/polydimethylsiloxane (PDMS) shell, with the outer diameter of 120 μm. By diluting PDMS to tune the thickness of liquid coating layer, droplets formation has been effectively prevented. The composite fiber exhibits a smooth surface structure and superior ML performances, including high brightness, excellent flexibility, and stability. In addition, a weft knitting textile fabricated by the continuous ML fiber can be easily delighted by manually stretching, and the ML fibers can emit visible signals upon human motion stimuli when woven into commercial cloth. Such continuous ultra-fine ML fibers are promising as wearable sensing devices for human motion detection and human–machine interactions.

KEYWORDS

mechanoluminescence, fiber, continuous synthesis, wearable textile

1 Introduction

Fiber-woven smart clothing has significant advantages in wearability and adaptability among various emerging wearable electronics [1, 2]. In recent years, functional-fiber-integrating textiles have demonstrated attractive applications, such as illumination and displays, human–machine interactions, energy harvesting and storage, multi-functional sensors, thermal management, and healthcare devices [3–8]. Mechanoluminescence (ML), the phenomenon of light emission triggered by mechanical force on a solid material, has attracted broad attention from researchers aiming for flexible wearable devices [9–11]. Fiber-shaped ML devices are promising components for the wearable light-emitting fabrics due to their excellent stretchability, biocompatibility, and inherent self-powering ability. However, continuous synthesis of fine fibers remains the critical challenge for the practical applications of functional ML fabrics [12, 13]. It is urgently needed to develop an effective synthesis approach for continuous and fine fibers.

Among all the ML/polymer composites developed with remarkable performance, ZnS:Cu/polydimethylsiloxane (PDMS) composites still are potential candidates in practical applications based on their high luminescence intensity, low detection limit, and excellent stretchability, so that most fiber-shaped ML devices are fabricated by ZnS:Cu phosphors and PMDS matrix [14–20]. To date, most fabrication processes of the ZnS:Cu/PDMS fibers can be divided into two categories, i.e., cutting ML composite films and dip-coating the luminescent layer on the elastic fibers. In the former approach, ZnS:Cu/PDMS films are cut into flat fibers, and then woven into a plain weave luminescent textile [21]; while for the latter method, an elastic fiber (as a core) is commonly dipped into a solution of ZnS:Cu/PDMS (as the luminescent layer) and pulled-out subsequently, and a highly stretchable and flexible ML fiber is obtained after curing [22]. Compared with the flat cutting fibers, dip-coating fibers with the co-axial structure and round cross-section deliver more uniformed tensile stress distribution, which is more suitable for wearable fabrics. More importantly, the dip-coating approach, already widely utilized for the continuous preparation of various functional fibers, is promising for industrial-scale production of ML fibers [23–25].

Flexibility is one of the crucial prerequisites for wearable textile [26–28]. However, all the luminescent fibers reported previously bear the undesirable large transactional diameters of or above sub-millimeter-scale, much larger than those of the commercial woven fibers of around tens of microns, which hardly satisfy the demand on flexibility [29, 30]. Thinner diameter allows the fiber to withstand a smaller curvature bending radius and much more complex deformation, thus reducing the diameters of both inner elastic core and outer luminescent shell might be an effective way to promote the flexibility of the luminescent fiber. However, when a fine elastic fiber (with a diameter of less than a few tens of micrometers) is adopted as the inner core, the viscous PDMS precursor gradually forms discrete droplets rather than a uniform

Address correspondence to Chong-Xin Shan, cxshan@zzu.edu.cn; Lin Dong, ldong@zzu.edu.cn

shell. The formation of the uniform structure is mainly caused by the Laplace pressure difference, which reduces the free surface area [31]. There is yet no practical technique to produce an even luminous coating on the fiber at the micron level, although some studies suggest that the even luminescent layer can be formed by reducing the thickness of the liquid layer [3, 32].

Therefore, innovated approach and reasonable selection of the elastic core are essential to realize continuous synthesis of flexible ML fiber. Here, a novel adhere-coating method is introduced instead of the common dip-coating method in order to fabricate fine ML fiber. In this approach, droplet formation is prevented by directly attaching the ZnS:Cu phosphors onto polyurethane (PU) fibers using PDMS adhesive to form a uniform luminescent layer. An ultra-fine ML fiber with a diameter of 120 μm is obtained, consisting of a fine PU elastic fiber and a thin ZnS:Cu/PDMS luminescent shell. Such fine fiber still maintains a remarkable ML intensity; besides, excellent flexibility and stability indicate their application potential in wearable ML textile. Moreover, the weft-knitted ML textile is obtained by the continuous ML fiber fabricated via a similar technique, which exhibits self-power displays during deformation. This continuous synthesis strategy is expected for mass production of flexible ML fibers and other functional fibers, which are essential for the commercialization of self-power display clothes.

2 Results and discussion

The schematic fabrication of the ultra-fine ML fiber is presented in Fig. 1(a), and the detailed process is provided in the Experimental section. The PU fiber is coated successively with dilute PDMS solution, ZnS:Cu particles, and a PDMS encapsulation layer to fabricate the ultrafine ML fiber. The scanning electron microscopy (SEM) morphologies of PU fiber, PU@PDMS/ZnS:Cu, and ML fiber are provided in Fig. 1(b). The PU fibers have a lateral size of ~ 100 μm, consisting of three individual PU silks with a diameter of ~ 50 μm. After attached with ZnS:Cu powders, the PU@PDMS/ZnS:Cu fiber shows an uneven surface, and these adhered particles are easy to fall off during deformation. The ZnS:Cu particles have a diameter of 10–30 μm, consisting of wurtzite and sphalerite phases with a weight ratio of about 71.9:28.1 (Fig. S1 in the Electronic Supplementary Material (ESM)). After encapsulated with the outer PDMS layer, the ML composite fiber develops an even and smooth surface, while the ZnS:Cu particles are fully embedded in the PDMS matrix. In addition, the PDMS encapsulation layer allows ML fiber to survive harsh chemical environments. The cross-sectional view shows a coaxial structure where the PU fiber is located at the center, which is surrounded by a PDMS/ZnS:Cu layer (Fig. 1(c)). The coaxial structure of ML fiber is also evidenced by fluorescence microscopy, as shown in the inset of Fig. 1(c). Upon higher magnified SEM observation shown in the pseudo-color image in Fig. 1(d), the ZnS:Cu particles (green part) are well embedded in the PDMS matrix (blue part) surrounding the PU fiber (yellow part). The thickness of the entire coating layer on the PU fiber is 20–50 μm, indicating that no more than two ZnS:Cu particles could be stacked at the same position.

By merits of both the slim PU core and thin PDMS/ZnS:Cu

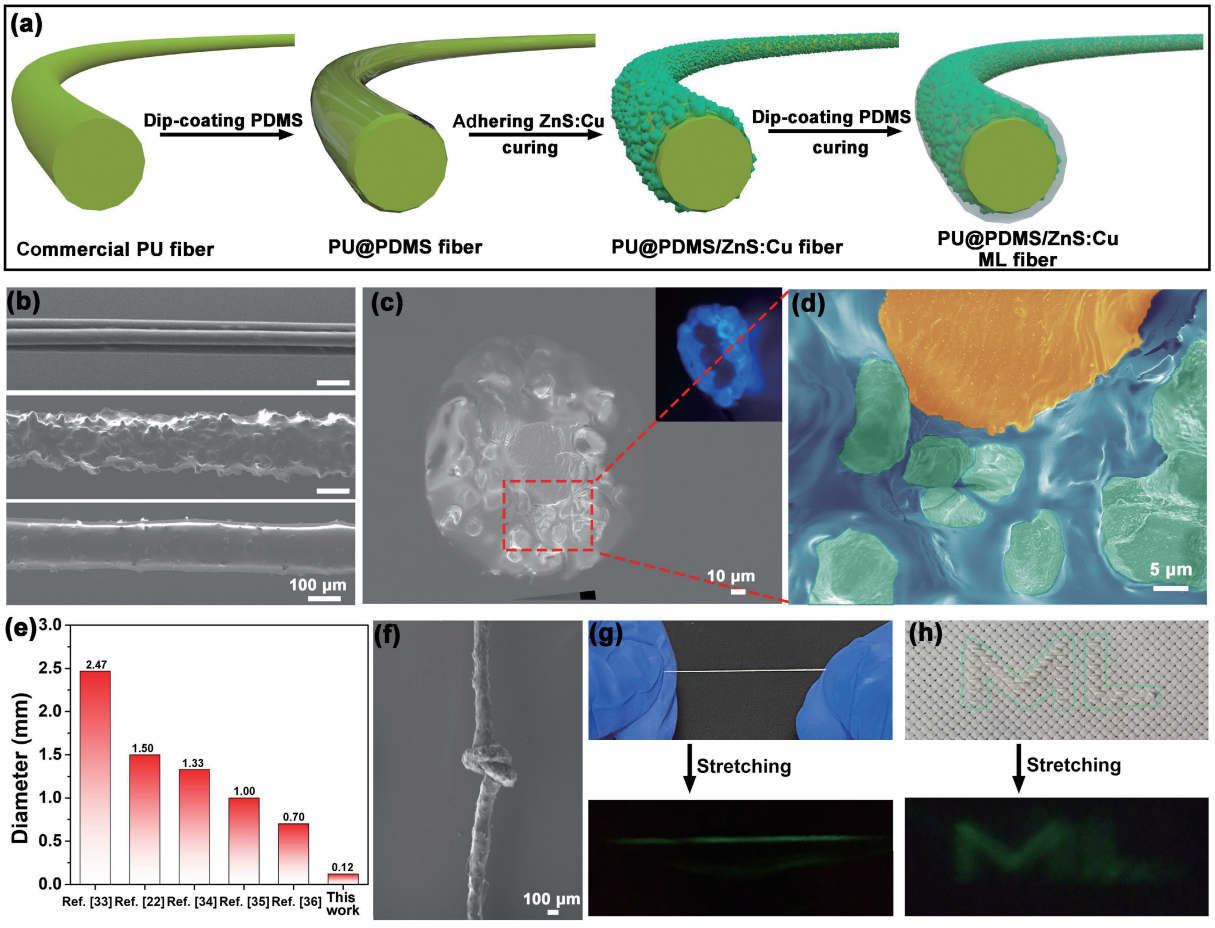

Figure 1 Fabrication and structure of ultra-fine ML fibers. (a) Schematic diagram showing the synthesis process of an ultra-fine ML fiber. (b) SEM images of a PU fiber, a PU@PDMS/ZnS:Cu fiber, and an ultra-fine ML fiber. (c) SEM image of an ultra-fine ML fiber at a cross-sectional view (inset: a fluorescence image of an ultra-fine ML fiber at a cross-sectional view). (d) High-magnification pseudo-color SEM image of ultra-fine ML fiber at a cross-sectional view (yellow: PU core; blue: PDMS matrix; green: ZnS:Cu phosphors). (e) The diameter of an ultra-fine ML fiber and those of previously prepared ML fibers. (f) SEM image of a tight ML fiber knot. (g) Photographs of an ultra-fine ML fiber and manually stretched ML-emitting fiber. (h) Photographs of ultra-fine ML fiber stitched into fabric and manually stretched ML-emitting embroidery.

coating layer, the ML fiber exhibits a thin diameter of about 120 μm, much smaller than that of most ML fiber ever reported (Fig. 1(e)) [22, 33–36]. The smaller diameter is favorable for flexibility, and allows the fiber to withstand much serious deformation. For instance, the fiber can be made into a tight knot without any observable cracks (Fig. 1(f)). These fine fibers still retain their ML characteristic, and the fiber demonstrates green light emission under repetitive stretching/releasing (Fig. 1(g)). Similar to commercial yarns, the ultra-fine fiber can be stitched into the fabric, while an "ML" pattern made of ML fiber can be lightened by manually stretching the embroidery (Fig. 1(h)).

In order to obtain the ultra-fine ML fibers, PDMS precursor mixture is diluted with n-hexane prior to the dip-coating process. The influence of the PDMS solution concentration on the resulting coating morphology is also investigated. Clearly, the fiber directly drawn from original PDMS mixtures bears a coating surface of separate droplets, with a size much larger than that of the PU fiber. As shown in Fig. 2(a), when the PDMS weight ratio decreases from 100 wt.% to 40 wt.%, the droplet size reduces significantly, and finally turns into an evenly distributed liquid shell when the PDMS weight ratio decreases to 20 wt.%. To investigate the evolution of vapor–liquid–solid interfacial tension when the mass fraction of PDMS decreases, contact angle measurement has been performed on flat PU surfaces, as shown in Fig. 2(b). The contact angle decreases from 57.13° gradually to 46.75°, 28.45°, and 23.57° for the PDMS weight ratio of 100 wt.%, 80 wt.%, 60 wt.%, and 40 wt.%, respectively; accordingly, the $d_{droplet}/d_{fiber}$ (a ratio of the diameter of the droplet to the diameter of PU fiber) decreases from 5.7 to 3.0, 2.0, and 1.4, respectively. It reveals that diluting PDMS solution is an effective way to produce fine fibers with smooth and consistent ML composite shells.

To shine further insight into the strategy to avoid the formation of droplets by diluting the PDMS solution, the transformation process of the sticky liquid film into the droplet is also investigated. The entire process can be simply divided into two stages: (i) the formation of a thin liquid film (shell) layer, and (ii) the shrinkage of the continuous film layer into regular wavy shape and so forth the separate droplets, as shown in Fig. 2(c). During the first stage of the liquid film formation, the thickness (e_0) of the liquid film is decided by the liquid surface tension (γ), the liquid viscosity (η), and the coating velocity (U) [31]

$$e_0 = \frac{b\mathrm{Ca}^{\frac{2}{3}}}{1-\mathrm{Ca}^{\frac{2}{3}}} \quad (1)$$

where b is the diameter of the inner PU fiber, and Ca, the capillary number, is defined as

$$\mathrm{Ca} = \frac{\eta U}{\gamma} \quad (2)$$

Hence, e_0 is positively correlated with η and U, and negatively correlated with γ.

For the later stage, Plateau–Rayleigh instability, induced by the surface tension to minimize the free surface area of liquid, plays an important role in the formation of droplets [37]. The pressure within the film includes both a hydrostatic contribution of order ρgR (ρ is the density of PDMS solution, g is the acceleration of gravity, and $R = b + e_0$) and a Laplace contribution of order γ/R. For a typical liquid cylinder with a diameter of about 100 μm, the

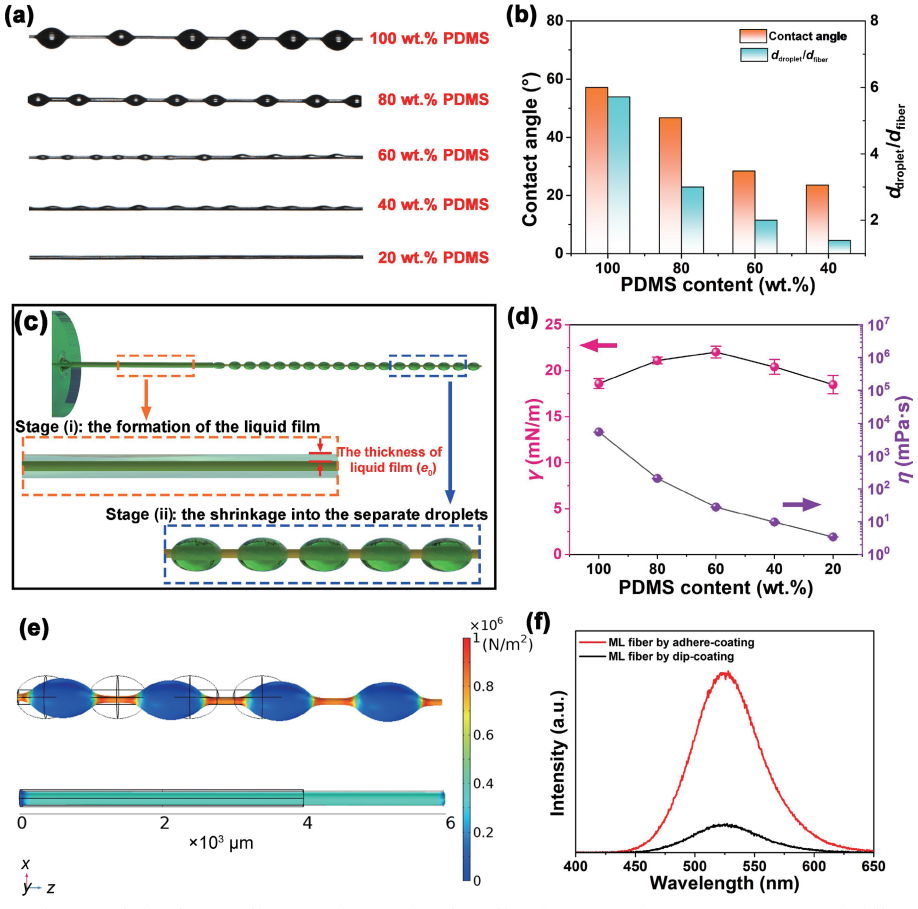

Figure 2 The formation mechanism of ultra-fine ML fibers. (a) Photographs of PU fiber dip-coating the PDMS precursors with different mass fractions. (b) The contact angle and the $d_{droplet}/d_{fiber}$ of PU fiber dip-coating the PDMS precursors with different mass fractions. (c) The schematic diagram of the transformation process of the sticky liquid film into the droplets. (d) The γ and η of the PDMS precursors with different mass fractions. (e) Mechanics simulation showing the stress concentration on the fibers with different structures under a tensile strain of 50% (black lines: the original states of the composite fibers). (f) ML spectra of the ML fibers fabricated by dip-coating and adhere-coating.

bond number (defined as the ratio of hydrostatic pressure to Laplace pressure difference) is only 0.01, indicating that gravity is negligible [31]. Under the Laplace pressure difference, a critical condition to coat the fiber with a stable film is obtained (details can be found in the ESM) as [32]

$$e_0 \leqslant (\sqrt{2}-1)b \quad (3)$$

Thus, whether the continuous liquid layer shrinks into spaced droplets relies mainly on the ratio of e_0 to b, and the lower thickness of PDMS coating formed in the first stage is favorable for its stability.

We have carried out a study on two key factors of PDMS solution, γ and η, which can influence the thickness of the film as above. As shown in Fig. 2(d) and Table S1 in the ESM, the surface tensions change slightly under different mass fractions of PDMS, while the liquid viscosity decreases abruptly from 5390 to 208.3, 28.2, 9.68, and 3.45 mPa·s with the small errors, for the PDMS weight ratios of 100 wt.%, 80 wt.%, 60 wt.%, 40 wt.%, and 20 wt.%, respectively. Therefore, the dilution of PDMS can significantly reduce the solution viscosity, resulting in a thin liquid film (according to Eqs. (1) and (2)), and further leading to the formation of an even and stable coating on the fiber (according to Eq. (3)). However, when the ZnS:Cu/PDMS mixture is diluted, the low viscosity of PDMS prevents the ZnS:Cu particles from dispersing in the PDMS solution homogeneously (Fig. S2 in the ESM), making it difficult to form a uniformed coating for subsequent dip-coating. In contrast, in the adhere-coating method, PDMS is not mixed with ZnS:Cu phosphors; instead, it serves as a bottom coating and encapsulation layer, which can act as a binder to adhere to the ZnS:Cu phosphors and protect them, respectively. Such novel strategy enables the homogenous loading ZnS:Cu phosphors while diluting PDMS to produce a thin layer.

In order to investigate the impact of the structure on ML performance, we fabricate two different ML composite fibers by common dip-coating and adhere-coating. The composite fiber prepared by adhere-coating shows a homogeneous structure when PDMS is diluted to a mass fraction of 40 wt.% (Fig. 1(b)), while the composite fiber obtained by dip-coating the un-diluted PDMS/ZnS:Cu solution shows an uneven pearl string structure (Fig. S3 in the ESM). The stress distributions of the ML composite fibers with these two structures are different under a tensile strain of 50% (Fig. 2(e)). The fiber with a homogeneous structure shows an even stress distribution, in which the stress is ~ 0.4 MPa all round; while the fiber with the pearl string structure exhibits stress concentrated between pearls, which prevents the embedded ZnS:Cu particles from being effectively forced. When ZnS:Cu particles are stimulated by an external force, plastic deformation leads to band bending and tunneling of trapped electrons at the shallow donor level to the conduction band. When these electrons recombine with holes, green emission occurs (Fig. S4 in the ESM) [38]. As a result, the composite fiber prepared by adhere-coating shows a higher integrated ML intensity over 5.5 times stronger than the composite fiber prepared by dip-coating (Fig. 2(f)). Such fine and homogeneous composite fiber with superior ML brightness is a promising candidate for wearable textiles. Besides, the ML composite fiber shows high stretchability (977%) and tensile strength (41.7 MPa), of the same level with PU fiber (1036% and 43.2 MPa) (Fig. S5 in the ESM). During the stretching test, the ZnS:Cu/PDMS luminescent layer maintains stable adhesion to the PU fiber under a strain of 100%, delivering an effective deformation range that could sustain the deformation caused by most human activities, and the small cracks appear when the strain increases to 150%–200% (Fig. S6 in the ESM). The ML composite fiber exhibits low residual strains of 0.8%, 2.2%, 4.5%, 6.4%, and 8.1%, under the loading–unloading testing at strains of 20%, 40%, 60%, 80%, and 100%, respectively, showing satisfactory elasticity and recoverability (Fig. S7 in the ESM). These excellent mechanical performances can meet more demands in practical applications.

In order to further explore the ML performances of these thin composite fiber, the ML spectra are measured under different applied strain of 10%–100% (Fig. 3(a)). The peaks are located at 520 nm and there is no shift under different strains. The integrated ML intensity increases linearly with strain ($y = 250.8x - 2282.8$, $R^2 = 0.995$), which would facilitate quantitative monitoring the applied strain (Fig. 3(b)). The ML brightness also has a linear relation to applied stress ($y = 8.3x - 3.5$, $R^2 = 0.984$) (Fig. S8 in the ESM). When the ML emissions are measured at different positions along the fiber under a tensile strain of 50%, similar ML intensities are observed, indicating that the ZnS:Cu phosphors are evenly distributed along the fiber (Fig. 3(c)). Due to the one-dimensional structure, which offers luminance in all directions, the ML brightness is almost independent of the observation angle (Fig. 3(d)). Additionally, it supports the homogeneous distribution of ZnS:Cu phosphors. Upon being stretched to a strain of 50% or bent into an angle of 180° for 5000 cycles, the composite fiber retains over 85% and 80% of initially brightness, respectively, at a tensile strain of 50% (Figs. 3(e) and 3(f)). Due to the excellent flexibility and recoverable ML performances, this remarkable stability has been achieved.

In order to bridge the gap between lab research and industry, the continuous synthesis of ML fiber is essential. To achieve the manufacture of meter-scale ML fiber, we have further developed a continuous synthesis technique (Fig. 4(a)). Typically, a fiber sequentially passes through the diluted PDMS precursors, the ZnS:Cu phosphor, the diluted PDMS precursors, the heating tube, the diluted PDMS precursors, and the heating tube, before being collected by a roller. By continuous dip-coating, adhering-coating, curing, dip-coating, curing, and final collecting successively, a continuous meter-scale ML fiber is obtained (Fig. S9 in the ESM). To tradeoff the ML-emitting brightness and flexibility, a PU fiber with a diameter of 200 μm is adopted to serve as inner core. Notably, during the synthesis process, the phosphors no longer need to be mixed with the solution, which facilitates to recycle and reuse of the phosphors. This flexible ML fiber can undertake complex deformations, and can also be woven into intricate textiles, such as weft-knit textiles, which feature abundant curved locations with significant curvature (Fig. 4(b)). Compared with plain biaxial weave fabrics, weft knit textile has less stress and is more comfortable under the same deformation, so it has been widely used in general apparel [39]. The weft knitted ML textile with a large size of 16 cm × 12 cm is shown in Fig. 4(c), in which interlaced and curved fiber can store mechanical energy, so that the ML textile may undergo complex deformation. As shown in Fig. 4(d), the ML textile exhibits satisfactory flexibility, and it can be folded or rolled without external force supporting and can be manually twisted into a tight rope. When manually stretched in a dark environment, the entire ML textile can be fully lightened (Fig. 4(e)). Besides, encapsulated with the hydrophobic PDMS, the ML textile can maintain its original brightness after washing for five rounds (Fig. 4(f)).

On the other hand, combining conventional fabrics and the single functional fibers is also an effective strategy to develop smart textiles. By integrating the ML fiber into the fabric, the visual functional fabric can be obtained, which can respond to deformations by ML-emitting (Figs. 1(h) and 5(a)). The photograph taken under ultraviolet (UV) irradiation (Fig. 5(b)) shows that the ML fiber is tightly woven into the conventional fabric without any cracks and deformations. Because of its fairly small diameter, the ML fiber exhibits excellent compatibility with

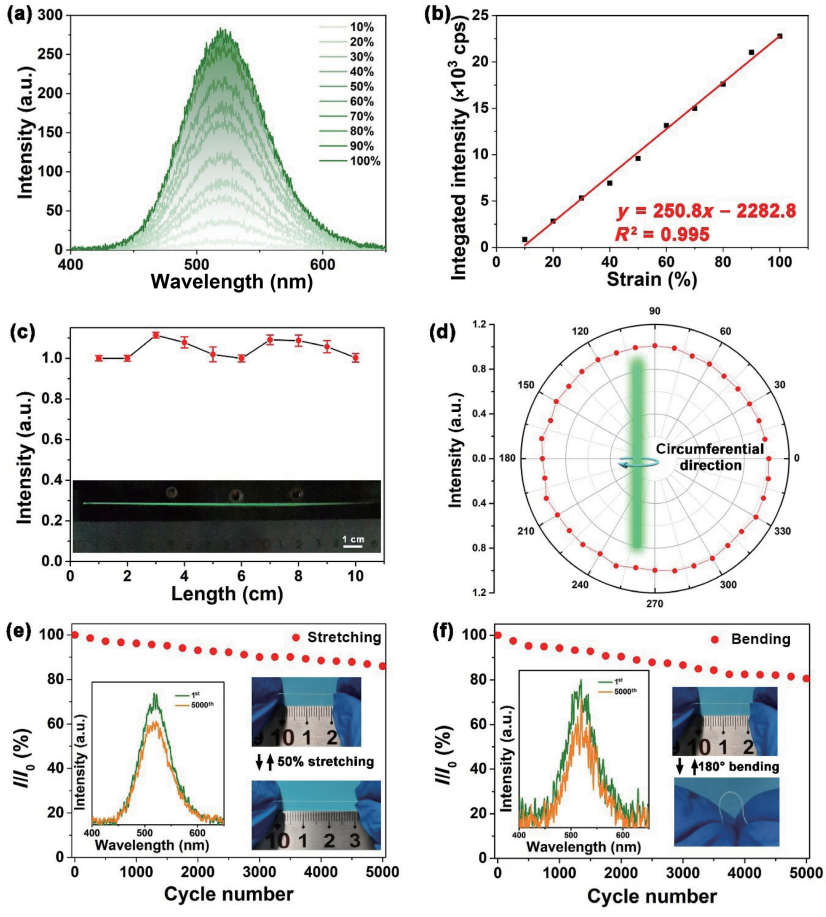

Figure 3 Mechanoluminescent performances. (a) ML spectra under different applied strains of 10%–100%. (b) Integrated intensity vs. applied strain of 10%–100%. (c) ML intensity distribution along the length of the fiber. (d) ML intensity distribution around the fiber. (e) ML intensity variation during ε = 50% long-term stretching cycles (inset: ML spectra for the first cycle and the 5000th cycle). (f) ML intensity variation under a strain of 50% after 180° bending cycles (inset: ML spectra of the origin fiber and the fiber after 5000 bending cycles).

the textile process technology. When the ML fiber is woven into commercial clothings (such as gloves, wrist guards, and kneepads), the obtained fabrics can serve as novel sensors for detecting human motion (Fig. 5(c)). To demonstrate the independent finger motion sensing, we knit the ML fiber into a commercial glove with a separate ML fiber on each finger (Fig. 5(d)). Making a fist causes the fiber to stretch and emit green light because of the bending finger. Interestingly, although the joint part of the finger can bend more than other parts, other parts can also be stretched, making practically every fiber delighted like a glowing skeleton of a hand. When a single finger is bent, the corresponding fiber is stretched and radiates optical signals, which can be used to qualitatively identify the force of the joint and realize the visualization of stress. The ML fiber knitted into clothes at the joints can also be stretched and emanate optical signals when bending the wrist, elbow, and knee, which can be utilized to discern between various human motions (Figs. 5(e)–5(g)). It is worth noting that the output optical signals increase with the increased bending angles when the ML fiber is attached to the corresponding positions: finger, wrist, elbow, and knee (Fig. S10 in the ESM). The ML fiber can provide self-power, real-time, and visual signals in response to stress or strain. The novel fiber-woven ML textile may thus be used as wearable sensors for human motion detection and human–machine interactions.

3 Conclusions

In this work, we fabricate a unique adhere-coating ML fiber with a small diameter. The PDMS is diluted to prevent the formation of droplets on the PU fiber surface, resulting in homogeneous ML fiber. The ultra-thin coaxial fiber exhibits superior ML intensity, flexibility, and stability. We further fabricate a weft knit textile from the continuous ML fiber, which can be easily delighted by manually stretching. The ML fibers sewn into the clothes can also serve as visual strain sensors when driven by human motions. Our ultra-thin ML fibers and ML textiles offer a promising platform to develop a new generation of self-powered wearable device.

4 Experimental

4.1 Fabrication of ultra-fine ML fiber

First, a PDMS precursor solution was prepared by mixing PDMS elastomer base and curing agent at a mass ratio of 10:1. Then, the PDMS precursor solution was diluted by n-hexane to mass fractions of 20 wt.%, 40 wt.%, 60 wt.%, and 80 wt.%. After that, a fine commercial PU fiber with a diameter of around 100 μm was first coated with diluted PDMS precursor solution by dip-coating. Un-cured PDMS coating served as adhesive and connected ZnS:Cu phosphors (Shanghai Keyan Optoelectronic Technology Co., Ltd.) onto PU fiber. After being cured at 80 °C for 30 min, the PU@PDMS/ZnS:Cu fiber was coated again with diluted PDMS precursor solution by dip-coating. After cured at 80 °C for 30 min, a ultra-fine ML fiber was obtained.

4.2 Continuous synthesis of ML fiber

To achieve the continuous synthesis, an automated apparatus was designed, containing PU fiber deed, dip-coating PDMS, heating, and collection roller controlled by motor. Typically, a continuous PU fiber was first immersed into diluted PDMS precursor solution

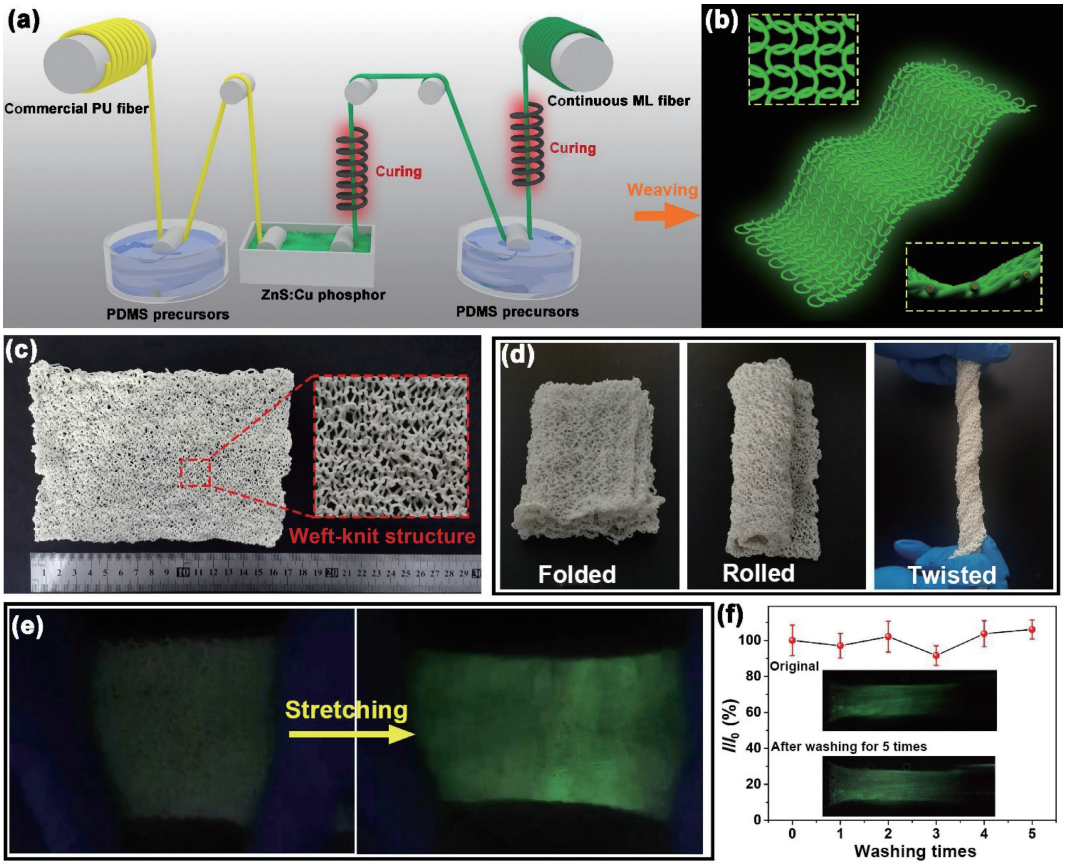

Figure 4 Continuous synthesis of fiber for ML textile. (a) Schematic diagram of the continuous synthesis of ML fiber. (b) Schematic diagram of ML textile with weft-knit structure. (c) Photographs of the continuous fiber woven ML textile with a large size of 16 cm × 12 cm (inset: a photograph of the ML textile with weft-knit structure). (d) Photographs of the ML textile subjected to deformations including folding, twisting and rolling. (e) Photographs of the ML textile and manually stretched ML-emitting textile. (f) ML intensity of ML textile after washing for five times.

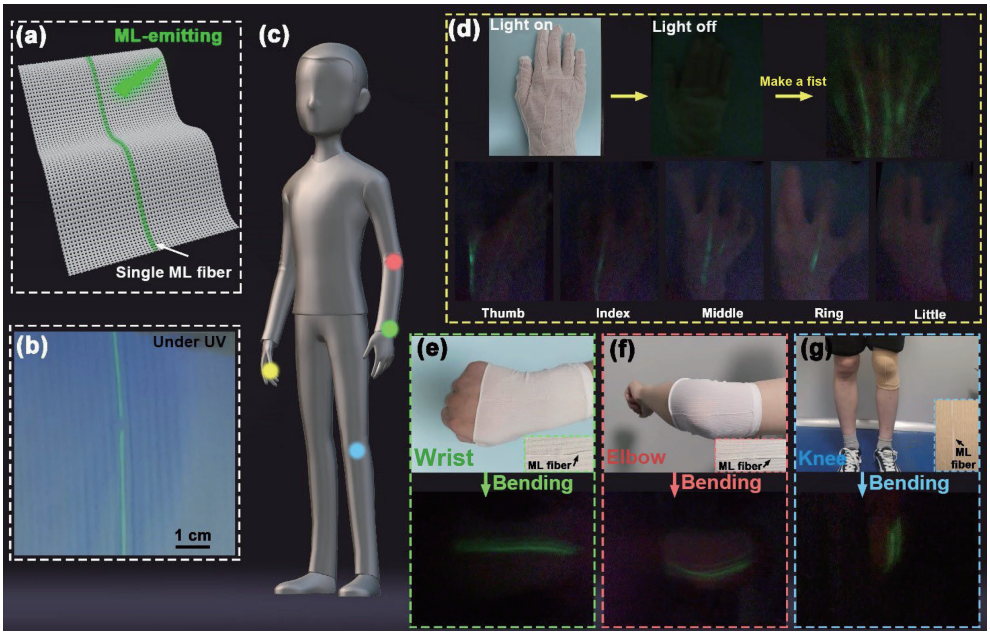

Figure 5 Single ML fiber woven with conventional fabrics for human motion detection. (a) Schematic diagram of a single ML fiber woven with the fabric. (b) Photograph of a single ML fiber woven with the fabric under UV irradiation. (c) Schematic diagram of ML fiber for human motion detection. (d) The optical signal generated by making a fist, and the corresponding generated optical signal of each finger. (e)–(g) The optical signals generated by bending wrist, elbow, and knee.

with a mass fraction of 40 wt.% and dragged out. Then, it was passed through a container of ZnS:Cu phosphors by pulleys, and passed through a heating tube to cure PDMS. After that, the fiber was immersed into diluted PDMS, dragged out, and passed through a heating tube, again, to form the encapsulation. Finally, the continuous ML fiber was collected by a roller.

4.3 Characterization and measurement

The morphologies of the samples were characterized by SEM (JEOL JSM-6700F). The crystal structures of the samples were studied via X-ray diffraction using Cu Kα1 radiation (λ = 1.5406 Å). The photoluminescence (PL) spectra were collected by a fluorescence spectrophotometer (F-7000, Hitachi). The contact

angles and the surface tensions were measured by a contact angle analyzer (Sindin SDC-200S). The viscosity measurement was carried out on a rotary viscosimeter (Lichen NDJ-8S). The mechanical properties were investigated on a single column tester (Instron 5943). The ML spectra were collected by a fiber optic spectrometer (Andor SR-500i-A). The participants wearing the ML textile for the wearable devices experiment were the first and third authors of this article. They understood the safety of the experiments and signed appropriate written, informed consents after explanation and discussion of their contents.

Acknowledgements

This work was supported by the National Natural Science Foundation of China (Nos. U22A2077 and 11974317), Henan Science Fund for Distinguished Young Scholars (No. 212300410020), Key Project of Henan Higher Education (No. 21A140001), and the Zhengzhou University Physics Discipline Improvement Program.

Electronic Supplementary Material: Supplementary material (further details of the material characterizations, ML properties, mechanical properties, and the details of on the evolution of droplet) is available in the online version of this article at https://doi.org/10.1007/s12274-023-5587-0.

References

[1] Chen, G. R.; Li, Y. Z.; Bick, M.; Chen, J. Smart textiles for electricity generation. *Chem. Rev.* **2020**, *120*, 3668–3720.

[2] Xiong, J. Q.; Chen, J.; Lee, P. S. Functional fibers and fabrics for soft robotics, wearables, and human–robot interface. *Adv. Mater.* **2021**, *33*, 2002640.

[3] Shi, X.; Zuo, Y.; Zhai, P.; Shen, J. H.; Yang, Y. Y. W.; Gao, Z.; Liao, M.; Wu, J. X.; Wang, J. W.; Xu, X. J. et al. Large-area display textiles integrated with functional systems. *Nature* **2021**, *591*, 240–245.

[4] Yan, W.; Noel, G.; Loke, G.; Meiklejohn, E.; Khudiyev, T.; Marion, J.; Rui, G. C.; Lin, J. N.; Cherston, J.; Sahasrabudhe, A. et al. Single fibre enables acoustic fabrics via nanometre-scale vibrations. *Nature* **2022**, *603*, 616–623.

[5] He, J. Q.; Lu, C. H.; Jiang, H. B.; Han, F.; Shi, X.; Wu, J. X.; Wang, L. Y.; Chen, T. Q.; Wang, J. J.; Zhang, Y. et al. Scalable production of high-performing woven lithium-ion fibre batteries. *Nature* **2021**, *597*, 57–63.

[6] Dong, K.; Peng, X.; Cheng, R. W.; Ning, C.; Jiang, Y.; Zhang, Y. H.; Wang, Z. L. Advances in high-performance autonomous energy and self-powered sensing textiles with novel 3D fabric structures. *Adv. Mater.* **2022**, *34*, 2109355.

[7] Wang, H. M.; Zhang, Y.; Liang, X. P.; Zhang, Y. Y. Smart fibers and textiles for personal health management. *ACS Nano* **2021**, *15*, 12497–12508.

[8] Libanori, A.; Chen, G. R.; Zhao, X.; Zhou, Y. H.; Chen, J. Smart textiles for personalized healthcare. *Nat. Electron.* **2022**, *5*, 142–156.

[9] Zhuang, Y. X.; Xie, R. J. Mechanoluminescence rebrightening the prospects of stress sensing: A review. *Adv. Mater.* **2021**, *33*, 2005925.

[10] Zhang, J. C.; Wang, X. S.; Marriott, G.; Xu, C. N. Trap-controlled mechanoluminescent materials. *Prog. Mater. Sci.* **2019**, *103*, 678–742.

[11] Wang, X. D.; Zhang, H. L.; Yu, R. M.; Dong, L.; Peng, D. F.; Zhang, A. H.; Zhang, Y.; Liu, H.; Pan, C. F.; Wang, Z. L. Dynamic pressure mapping of personalized handwriting by a flexible sensor matrix based on the mechanoluminescence process. *Adv. Mater.* **2015**, *27*, 2324–2331.

[12] Liao, M.; Wang, C.; Hong, Y.; Zhang, Y. F.; Cheng, X. L.; Sun, H.; Huang, X. L.; Ye, L.; Wu, J. X.; Shi, X. et al. Industrial scale production of fibre batteries by a solution-extrusion method. *Nat. Nanotechnol.* **2022**, *17*, 372–377.

[13] Wang, L.; Fu, X. M.; He, J. Q.; Shi, X.; Chen, T. Q.; Chen, P. N.; Wang, B. J.; Peng, H. S. Application challenges in fiber and textile electronics. *Adv. Mater.* **2020**, *32*, 1901971.

[14] Xiong, P. X.; Peng, M. Y.; Yang, Z. M. Near-infrared mechanoluminescence crystals: A review. *iScience* **2021**, *24*, 101944.

[15] Ning, J. J.; Zheng, Y. T.; Ren, Y. T.; Li, L. P.; Shi, X. Q.; Peng, D. F.; Yang, Y. M. MgF_2:Mn^{2+}: Novel material with mechanically-induced luminescence. *Sci. Bull.* **2022**, *67*, 707–715.

[16] Peng, D. F.; Jiang, Y.; Huang, B. L.; Du, Y. Y.; Zhao, J. X.; Zhang, X.; Ma, R. H.; Golovynskyi, S.; Chen, B.; Wang, F. A ZnS/CaZnOS heterojunction for efficient mechanical-to-optical energy conversion by conduction band offset. *Adv. Mater.* **2020**, *32*, 1907747.

[17] Li, C. H.; He, Q. G.; Wang, Y.; Wang, Z. J.; Wang, Z. J.; Annapooranan, R.; Latz, M. I.; Cai, S. Q. Highly robust and soft biohybrid mechanoluminescence for optical signaling and illumination. *Nat. Commun.* **2022**, *13*, 3914.

[18] Deng, Y.; Wei, J. Y.; Sun, J. L.; Zhang, Y. A.; Dong, L.; Shan, C. X. Enhancing the mechanoluminescence of traditional ZnS:Mn phosphors via Li^+ co-doping. *J. Lumin.* **2020**, *225*, 117364.

[19] Du, Y. Y.; Jiang, Y.; Sun, T. Y.; Zhao, J. X.; Huang, B. L.; Peng, D. F.; Wang, F. Mechanically excited multicolor luminescence in lanthanide ions. *Adv. Mater.* **2019**, *31*, 1807062.

[20] Qasem, A.; Xiong, P. X.; Ma, Z. J.; Peng, M. Y.; Yang, Z. M. Recent advances in mechanoluminescence of doped zinc sulfides. *Laser Photonics Rev.* **2021**, *15*, 2100276.

[21] Park, H. J.; Kim, S.; Lee, J. H.; Kim, H. T.; Seung, W.; Son, Y.; Kim, T. Y.; Khan, U.; Park, N. M.; Kim, S. W. Self-powered motion-driven triboelectric electroluminescence textile system. *ACS Appl. Mater. Interfaces* **2019**, *11*, 5200–5207.

[22] Zhang, J.; Bao, L. K.; Lou, H. Q.; Deng, J.; Chen, A.; Hu, Y. J.; Zhang, Z. T.; Sun, X. M.; Peng, H. S. Flexible and stretchable mechanoluminescent fiber and fabric. *J. Mater. Chem. C* **2017**, *5*, 8027–8032.

[23] Ye, C.; Ren, J.; Wang, Y. L.; Zhang, W. W.; Qian, C.; Han, J.; Zhang, C. X.; Jin, K.; Buehler, M. J.; Kaplan, D. L. et al. Design and fabrication of silk templated electronic yarns and applications in multifunctional textiles. *Matter* **2019**, *1*, 1411–1425.

[24] Gao, Y. Y.; Li, Z. H.; Xu, B. G.; Li, M. Q.; Jiang, C. H. Z.; Guan, X. Y.; Yang, Y. J. Scalable core-spun coating yarn-based triboelectric nanogenerators with hierarchical structure for wearable energy harvesting and sensing via continuous manufacturing. *Nano Energy* **2022**, *91*, 106672.

[25] Fan, H. W.; Li, K. R.; Liu, X. L.; Xu, K. X.; Su, Y.; Hou, C. Y.; Zhang, Q. H.; Li, Y. G.; Wang, H. Z. Continuously processed, long electrochromic fibers with multi-environmental stability. *ACS Appl. Mater. Interfaces* **2020**, *12*, 28451–28460.

[26] Wang, C. F.; Wang, C. H.; Huang, Z. L.; Xu, S. Materials and structures toward soft electronics. *Adv. Mater.* **2018**, *30*, 1801368.

[27] Zhang, Z. T.; Wang, W. C.; Jiang, Y. W.; Wang, Y. X.; Wu, Y. L.; Lai, J. C.; Niu, S. M.; Xu, C. Y.; Shih, C. C.; Wang, C. et al. High-brightness all-polymer stretchable LED with charge-trapping dilution. *Nature* **2022**, *603*, 624–630.

[28] Niu, S. M.; Matsuhisa, N.; Beker, L.; Li, J. X.; Wang, S. H.; Wang, J. C.; Jiang, Y. W.; Yan, X. Z.; Yun, Y.; Burnett, W. et al. A wireless body area sensor network based on stretchable passive tags. *Nat. Electron.* **2019**, *2*, 361–368.

[29] Choi, H. W.; Shin, D. W.; Yang, J. J.; Lee, S.; Figueiredo, C.; Sinopoli, S.; Ullrich, K.; Jovančić, P.; Marrani, A.; Momentè, R. et al. Smart textile lighting/display system with multifunctional fibre devices for large scale smart home and IoT applications. *Nat. Commun.* **2022**, *13*, 814.

[30] Kwon, S.; Hwang, Y. H.; Nam, M.; Chae, H.; Lee, H. S.; Jeon, Y.; Lee, S.; Kim, C. Y.; Choi, S.; Jeong, E. G. et al. Recent progress of fiber shaped lighting devices for smart display applications-a fibertronic perspective. *Adv. Mater.* **2020**, *32*, 1903488.

[31] Gennes, P.; Brochard-Wyart, F.; Quéré, D. *Capillarity and Wetting Phenomena*: *Drops*, *Bubbles*, *Pearls*, *Waves*; Springer: Berlin, 2004.

[32] Wang, Y.; Ren, J.; Ye, C.; Pei, Y.; Ling, S. J. Thermochromic silks for temperature management and dynamic textile displays. *Nano-Micro Lett.* **2021**, *13*, 72.

[33] He, M.; Du, W. W.; Feng, Y. M.; Li, S. J.; Wang, W.; Zhang, X.; Yu, A. F.; Wan, L. Y.; Zhai, J. Y. Flexible and stretchable triboelectric nanogenerator fabric for biomechanical energy harvesting and self-powered dual-mode human motion monitoring. *Nano Energy* **2021**, *86*, 106058.
[34] Liang, H. H.; He, Y. C.; Chen, M. H.; Jiang, L. C.; Zhang, Z. S.; Heng, X. B.; Yang, L.; Hao, Y. P.; Wei, X. M.; Gan, J. L. et al. Self-powered stretchable mechanoluminescent optical fiber strain sensor. *Adv. Intell. Syst.* **2021**, *3*, 2100035.
[35] Yang, W. F.; Gong, W.; Gu, W.; Liu, Z. X.; Hou, C. Y.; Li, Y. G.; Zhang, Q. H.; Wang, H. Z. Self-powered interactive fiber electronics with visual-digital synergies. *Adv. Mater.* **2021**, *33*, 2104681.
[36] Jeong, S. M.; Song, S.; Seo, H. J.; Choi, W. M.; Hwang, S. H.; Lee, S. G.; Lim, S. K. Battery-free, human-motion-powered light-emitting fabric: Mechanoluminescent textile. *Adv. Sustainable Syst.* **2017**, *1*, 1700126.
[37] Mead-Hunter, R.; King, A. J. C.; Mullins, B. J. Plateau Rayleigh instability simulation. *Langmuir* **2012**, *28*, 6731–6735.
[38] Hou, B.; Yi, L. Y.; Li, C.; Zhao, H.; Zhang, R.; Zhou, B.; Liu, X. G. An interactive mouthguard based on mechanoluminescence-powered optical fibre sensors for bite-controlled device operation. *Nat. Electron.* **2022**, *5*, 682–693.
[39] Wu, Y. Y.; Mechael, S. S.; Carmichael, T. B. Wearable e-textiles using a textile-centric design approach. *Acc. Chem. Res.* **2021**, *54*, 4051–4064.